Supplementary Information for "Forecasting the location and timing of eruptive vents with a particle filter"

L. Zuccali [*α, β], V. Pinel [†β], and Y. Yan[α]

[α] LISTIC, Université Savoie Mont Blanc, Annecy, France.

[β] Univ. Grenoble Alpes, Univ. Savoie Mont Blanc, CNRS, IRD, Univ. Gustave Eiffel, ISTerre, Grenoble, France.

Non Technical Summary

In order to improve predictions regarding the location and timing of future eruptions, we propose a new strategy that combines dynamic magma propagation models with ground surface displacements recorded by volcanic monitoring networks. The strategy is based on data assimilation commonly used for weather forecasting. In the case of tracking magma propagation at depth, the main difficulty lies in the lack of direct observations of the magma's position. By testing our data assimilation strategy for predicting eruptions on synthetic data, we have shown that it is possible to accurately predict the position of the future eruptive vent and obtain information on the volume, location and physical properties of the magma stored within the crust. These initial results are promising in terms of the potential for improving volcanic risk management in the near future through data assimilation, but they must first be confirmed using real data.

[*] zuccali.lea@gmail.com
[†] Virginie.Pinel@univ-smb.fr

1 Stress field in 2D plane strain approximation for a caldera under extensional stress field

We consider the z-axis to be oriented upwards with z equal to zero at the surface (see Figure S1) and adopt the convention that a tensile stress is negative. Following Watanabe et al. 2002, the stress field due to a constant surface unloading of amplitude P_l applied at the surface for $-R_{cal} < x < R_{cal}$ is given by:

$$\begin{aligned}
\sigma_{xx} &= -\frac{P_l}{\pi}\left[(\theta_1 - \theta_2) + \frac{(x+R_{cal})z}{(x+R_{cal})^2+z^2} - \frac{(x-R_{cal})z}{(x-R_{cal})^2+z^2}\right] \\
\sigma_{zz} &= -\frac{P_l}{\pi}\left[(\theta_1 - \theta_2) - \frac{(x+R_{cal})z}{(x+R_{cal})^2+z^2} + \frac{(x-R_{cal})z}{(x-R_{cal})^2+z^2}\right] \\
\sigma_{xz} &= \frac{P_l}{\pi}\frac{z^2(r_2^2 - r_1^2)}{r_1^2 r_2^2}
\end{aligned} \tag{S1}$$

θ_1 and θ_2 are the angles represented in Figure S1 and given by:

$$\theta_1 = \arctan\left(\frac{-z}{x - R_{cal}}\right)$$
$$\theta_2 = \arctan\left(\frac{-z}{x + R_{cal}}\right)$$

with r_1 et r_2 defined as :

$$r_1^2 = (x - R_{cal})^2 + z^2$$
$$r_2^2 = (x + R_{cal})^2 + z^2$$

In order to take the extension into account, we modify the expression of the horizontal stress field σ_{xx}, which becomes:

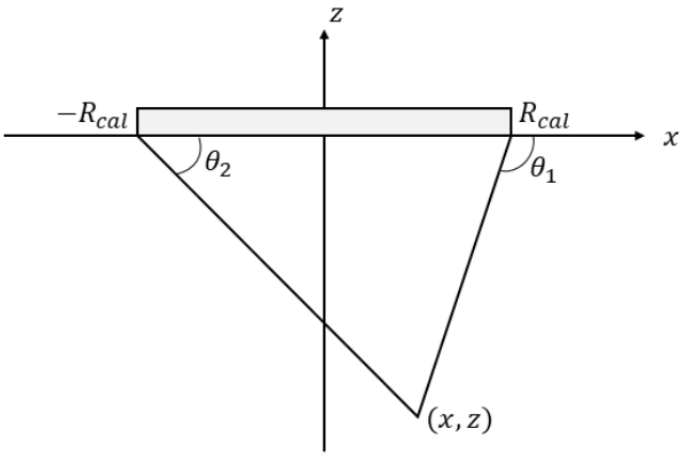


Figure S1: Model geometry.

$$\sigma_{xx} = -\frac{P_l}{\pi}\left[(\theta_1 - \theta_2) + \frac{(x+R_{cal})z}{(x+R_{cal})^2+z^2} - \frac{(x-R_{cal})z}{(x-R_{cal})^2+z^2}\right] - R * P_l \tag{S2}$$

2 Derivation of the magmatic intrusion length and opening from the initial model parameters

In Smittarello et al. 2021, equation 11 gives the volume of fluid inside a buoyant crack filled with a non viscous fluid, a so-called Weertman crack, which can be expressed as:

$$V = \alpha(1-\nu^2)\frac{\Delta\rho g}{E}L^4 \tag{S3}$$

where L is the length of the crack, E and ν are, respectively, the Young's modulus and Poisson's ratio of the surrounding medium, $\Delta\rho$ is the density contrast between the surrounding medium and the fluid, g is the acceleration due to gravity, and α equal to 0.25 from experimental data (Figure 9 of Smittarello et al. 2021). The magma driving pressure P_m can be expressed following Maccaferri et al. 2019 by:

$$P_m = \frac{\Delta\rho g L}{4} \tag{S4}$$

As $P_m = \gamma P_l$, we have:

$$\Delta\rho g L = 4\gamma P_l \tag{S5}$$

Combining equations (S3) and (S5) we obtain:

$$L = \left(\frac{VE}{\gamma(1-\nu^2)P_l}\right)^{1/3} \tag{S6}$$

We define an average opening w as:

$$w = A/L, \tag{S7}$$

where A is the cross-sectional area of the fissure (along the vertical plane x,y) given by equation 10 of Smittarello et al. 2021 for a crack filled with a non-viscous fluid:

$$A = \frac{\pi(1-\nu^2)}{8}\frac{\Delta\rho g}{E}L^3 \tag{S8}$$

Combining equations (S3), (S7) and (S8) we obtain the following expression for the mean opening:

$$w = \frac{\pi}{2}\frac{V}{L^2} \tag{S9}$$

3 The Stochastic Universal Sampling (SUS) algorithm

Let's consider a set of n particles $p_1, p_2, \ldots, p_n$ with weights $w_1, w_2, \ldots, w_n$. The algorithm works as follows (illustrated in Figure S2):

1. Initialization: marker distance is defined as $d = \frac{1}{n}$
2. Selection pointer positions: a random number $s \in [0, d]$ is defined as the starting point. Then the selection pointer positions are $s, s+d, s+2d, \ldots, s+(n-1)d$.

3. A cumulative sum S_c is defined as the cumulative sum of the particles weights initialized to w_1, and i is an index initialized to 0.

4. For each selection pointer p:

   - If $p > S_c$, i is incremented and S_c is updated by adding w_i.
   - p_i is added to the selection.
   - Move to the next pointer.

5. Return the list of n selected particles.

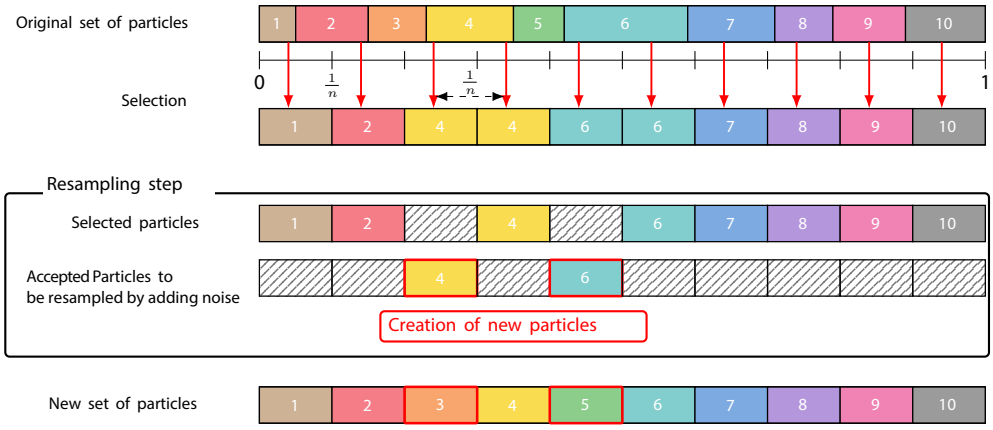


Figure S2: Principle of the Stochastic Universal Sampling algorithm.

4 Retrieval of parameters R and γ

The retrieval of parameters R and γ is performed by ensuring consistency with the intrusion position and dip. We calculate the orientation of the effective unit vector $\overrightarrow{U_{1,eff}}$ in each grid position for 399 possible combinations of parameters R and γ (R being between 0 and 1, with a step of 0.05, and γ between 0.05 and 0.95 with a step of 0.05). For each resampled particle, we calculate the likelihood of all combinations of parameters R and γ given the intrusion position and dip, and we randomly select one combination among the 10% more likely combinations. This strategy is illustrated for the specific case of a particle located at x=-5123 m and z=-8211 m and having a dip δ of 1.48 rad (magmatic intrusion close to the vertical), as shown in Figure S3.

We also tested the impact of the number of combinations retained in the selection by varying the percentage of the most probable combinations, from 1% to 30%. Figure S4 shows that this factor has no significant effect on our results.

5 Testing the direct perturbation of primary parameters

We carried out some preliminary tests by adding noise directly to the primary parameters rather than to the Okada parameters during particle resampling. In this approach, the step of retrieving the primary parameters from the Okada parameters was therefore skipped, and a standard propagation was carried out from the initial position of the particles (time t = 0) to the

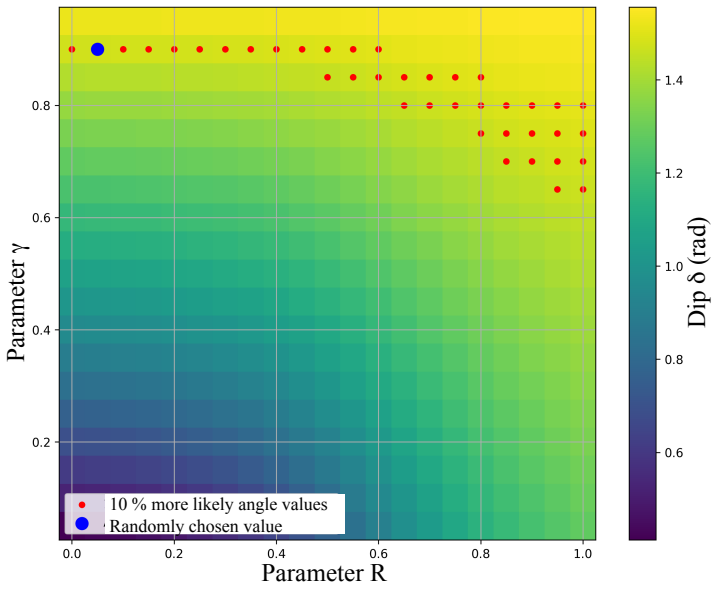


Figure S3: Values of the dip δ for different combinations of parameters R and γ estimated at position $x = -5123$ m and $z = -8211m$ with 10% of the most likely values shown as red dots and the randomly selected values shown with a blue dot.

current time step. The new primary parameters $x_{o,new}$, $z_{o,new}$, R_{new}, γ_{new}, μ_{new}, E_{new} and V_{new} of resampled particles are obtained by adding random noise to primary parameter of an accepted particle $x_{o,ac}$, $z_{o,ac}$, R_{ac}, γ_{ac}, μ_{ac}, E_{ac} and V_{ac} as described in Table S1.

Results obtained are presented in figure S5. A rapid decrease in the spread of the distribution prevents convergence towards the synthetic truth.

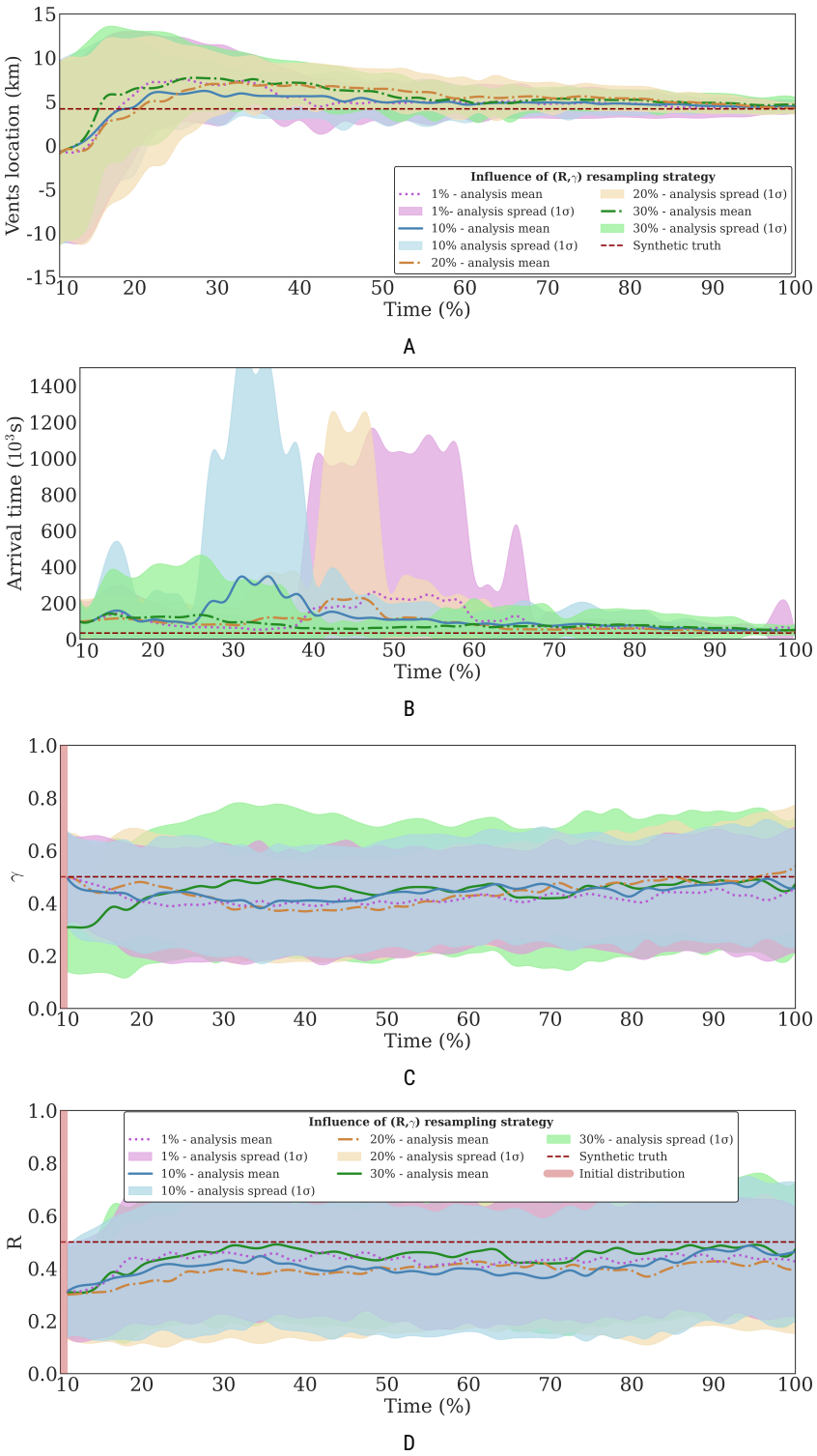


Figure S4: Influence of the percentage of more likely combinations considered to randomly pick one combination. Evolution over time of [A] the vent location prediction , [B] the arrival time prediction, [C] parameter γ and [D] parameter R. Lines are for the mean of the analyses and shaded areas correspond to the spread (1 σ) of the analyses. The theoretical value is represented by the red dashed line.

6 Effect of the spatial resolution of the grid on the prediction

Table S1: Characteristics of the noise added to the primaty parameters of an accepted particle.

Parameter	Value	Distribution	Units
$x_{o,new}$	$x_{o,new} = x_{o,ac} + \epsilon_x$	$\epsilon_x \sim \mathcal{U}(-500, 500)$	m
$z_{o,new}$	$z_{o,new} = z_{o,ac} + \epsilon_z$	$\epsilon_z \sim \mathcal{U}(-500, 500)$	m
R_{new}	$R_{new} = R_{ac} + \epsilon_R$	$\epsilon_R \sim \mathcal{U}(-0.1, 0.1)$	-
γ_{new}	$\gamma_{new} = \gamma_{ac} + \epsilon_\gamma$	$\epsilon_\gamma \sim \mathcal{U}(-0.1, 0.1)$	-
μ_{new}	$\mu_{new} = \mu_{ac} + \epsilon_\mu$	$\epsilon_\mu \sim \mathcal{U}(-50, 50)$	Pa.s
E_{new}	$E_{new} = E_{ac} + \epsilon_E$	$\epsilon_E \sim \mathcal{U}(-0.5, 0.5)$	GPa
V_{new}	$V_{new} = V_{ac} + \epsilon_V$	$\epsilon_V \sim \mathcal{U}(-0.01, 0.01)$	km^3

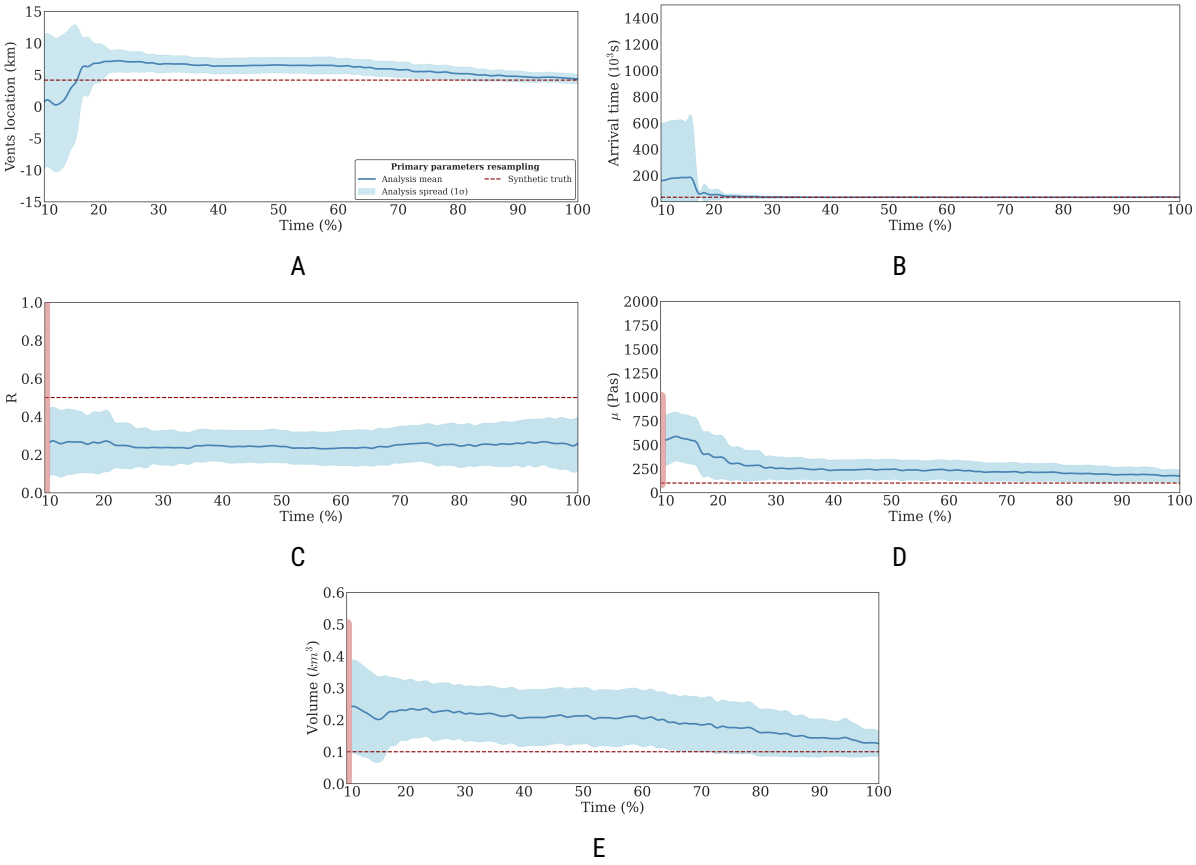


Figure S5: Predictions of the particle filter when primary parameters are directly perturbed during the resampling (spatial step of 100 m, $n = 100$, $\Delta w = 1\%$, $N_o = 600$). [A] Evolution over time of the prediction of eruptive vent location. [B] Evolution over time of the prediction of time of eruption t_e. [C] Evolution of the parameter R. [D] Evolution of the magma viscosity. [E] Evolution of the magma volume. The blue solid line correspond to the mean of the analyses. The blue shaded areas correspond to the 1σ spread of the analyses. The theoretical value (synthetic truth) is represented by the red dashed line. The thick pink line on the Y-axis corresponds to the initial range of the parameter (see Table 1 of the manuscript).

7 Influence of the number of particles, the duration of the assimilation window and the number of observations on the evolution of the parameters

Further results, illustrating how the parameters vary with respect to the number of particles, the duration of the assimilation window and the number of observations, are presented in Figures S7, S8 and S9 respectively.

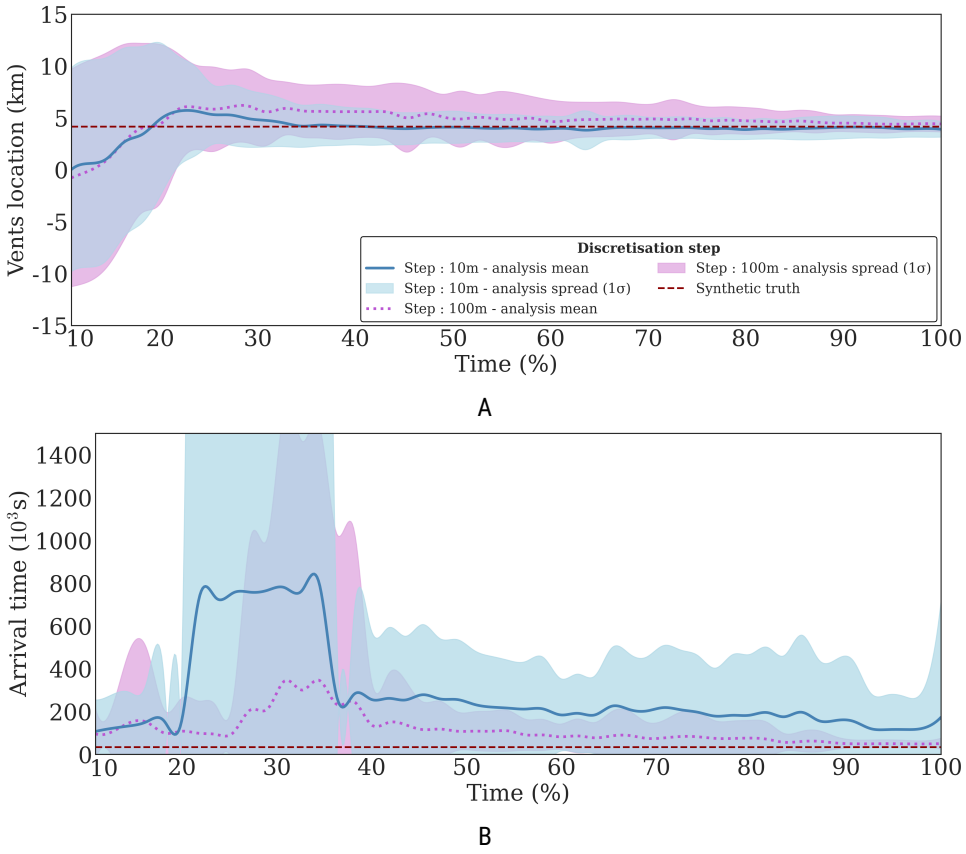


Figure S6: Predictions of the particle filter as a function of the grid spatial resolution (spatial step of 10 m is compared to the reference case of 100 m, $n = 100$, $\Delta w = 1\%$, $N_o = 600$). [A] Evolution over time of the prediction of eruptive vent location. [B] Evolution over time of the prediction of time of eruption t_e. The blue solid and pink dotted lines correspond to the mean of the analyses, for respectively, the 10 and 100 m grid step. The blue and pink shaded areas correspond to the 1σ spread of the analyses. The theoretical value (synthetic truth) is represented by the red dashed line.

8 Radar diagrams

In the following, we present the evolution over time of the Normalized Mean Absolute Error, $NMAE$, of the seven initial model parameters in different experiments. For a given parameter P, $NMAE$ is calculated as follows:

$$NMAE = \frac{1}{n}\sum_{i=1}^{n}\left(\frac{|P_{truth} - P_i|}{Max_P}\right) \tag{S10}$$

with P_{truth}, the true value of the parameter P, i.e. the value chosen to produce the synthetic truth and given in Table 2 of the main manuscript, P_i the value of parameter P for the particle number i and Max_P the maximum value of $|P_{truth} - P_i|$ with $i = 1, 2, ..., n$. The initial value of $NMAE$ depends on the position of the true value within the parameter range, but since we use a uniform distribution for the parameters and the true values lie within the parameter range, this initial value is close to 0.5. Any decrease in the $NMAE$ over time, i.e. an expansion of the colored area towards the outer circle, corresponds to an improvement in the parameter estimation.

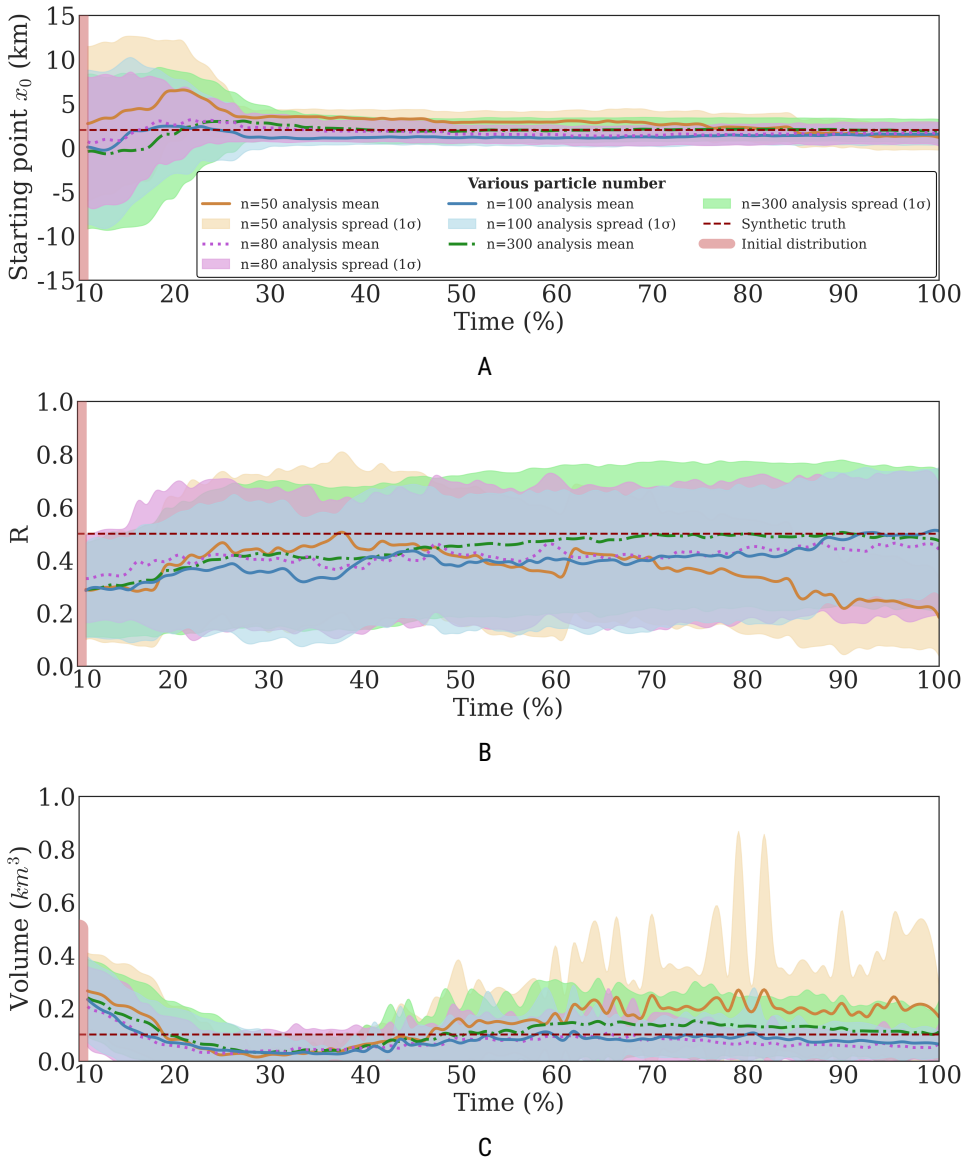


Figure S7: Parameters of the particle filter for 4 different numbers of particles: $n = 50$ in red/orange, $n = 80$ in purple, $n = 100$ in blue (reference case shown in Figure 8 of the manuscript and $n = 300$ in green. For each case $\Delta w = 1\%$ and $N_o = 600$. Evolution over time of [A] starting position x_0, [B] parameter R and [C] magma volume V. Lines are for the mean of the analyses and shaded areas correspond to the spread (1 σ) of the analyses. The thick pink line on the Y-axis corresponds to the initial range of the parameter (see Table 1 of the manuscript). The theoretical value is represented by the red dashed line.

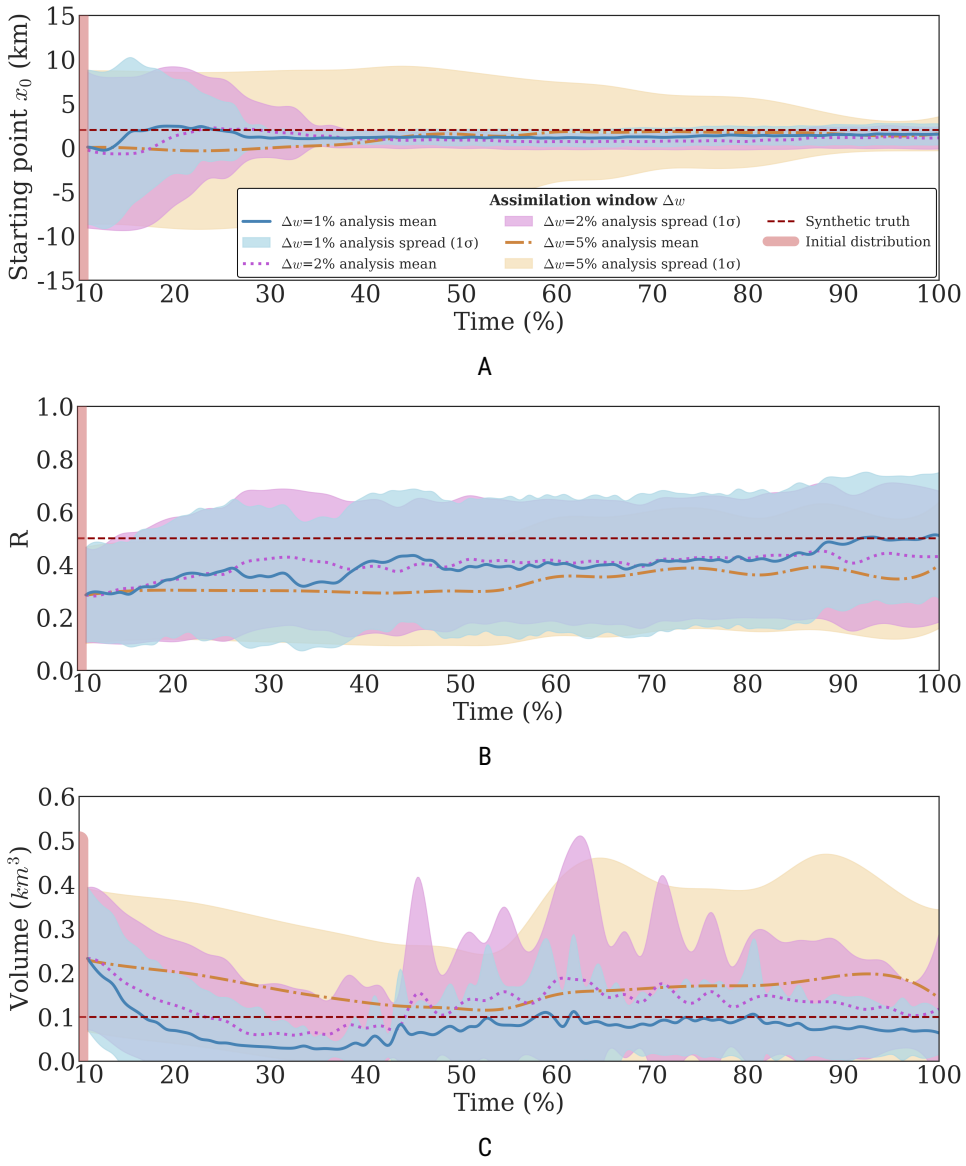


Figure S8: Parameters of the particle filter for 3 different assimilation windows: $\Delta w = 5\%$ in red/orange, $\Delta w = 2\%$ in purple and $\Delta w = 1\%$ in blue (reference case shown in Figure 8 of the manuscript. For each case $n = 100$ and $N_o = 600$. Evolution over time of [A] starting position x_0, [B] parameter R, and [C] magma volume V. Lines are for the mean of the analyses and shaded areas correspond to the spread (1 σ) of the analyses. The thick pink line on the Y-axis corresponds to the initial range of the parameter (see Table 1 of the manuscript). The theoretical value is represented by the red dashed line.

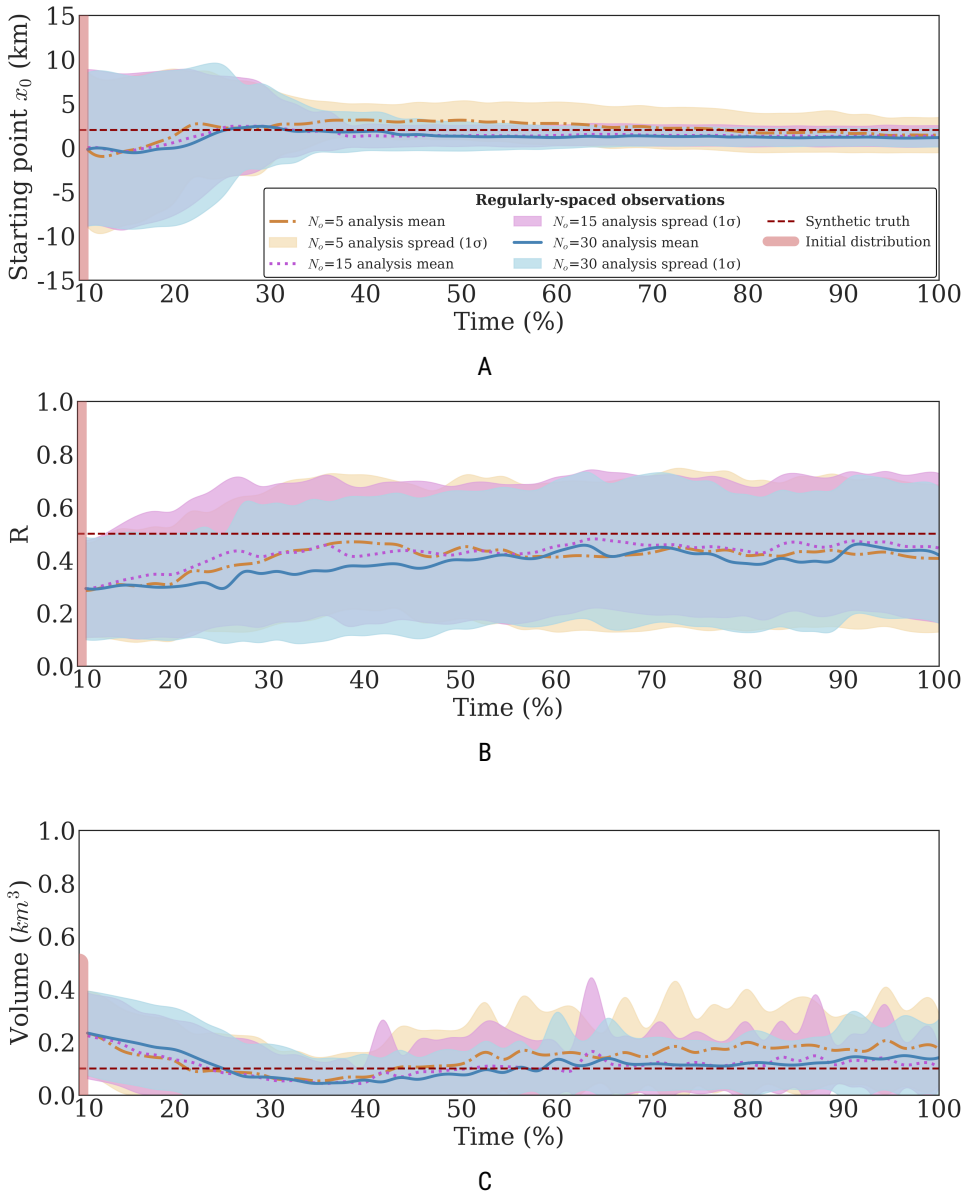


Figure S9: Parameters of the particle filter for 3 different numbers of regularly spaced observations: $N_o = 5\%$ in red/orange, $N_o = 15$ in purple and $N_o = 30$ in blue. For each case $n = 100$ and $\Delta w = 2\%$. Evolution over time of [A] starting position x_0, [B] parameter R and [C] magma volume V. Lines are for the mean analyses and shaded areas correspond to the spread (1 σ) of the analyses. The thick pink line on the Y-axis corresponds to the initial range of the parameter (see Table 1 of the manuscript). The theoretical value is represented by the red dashed line.

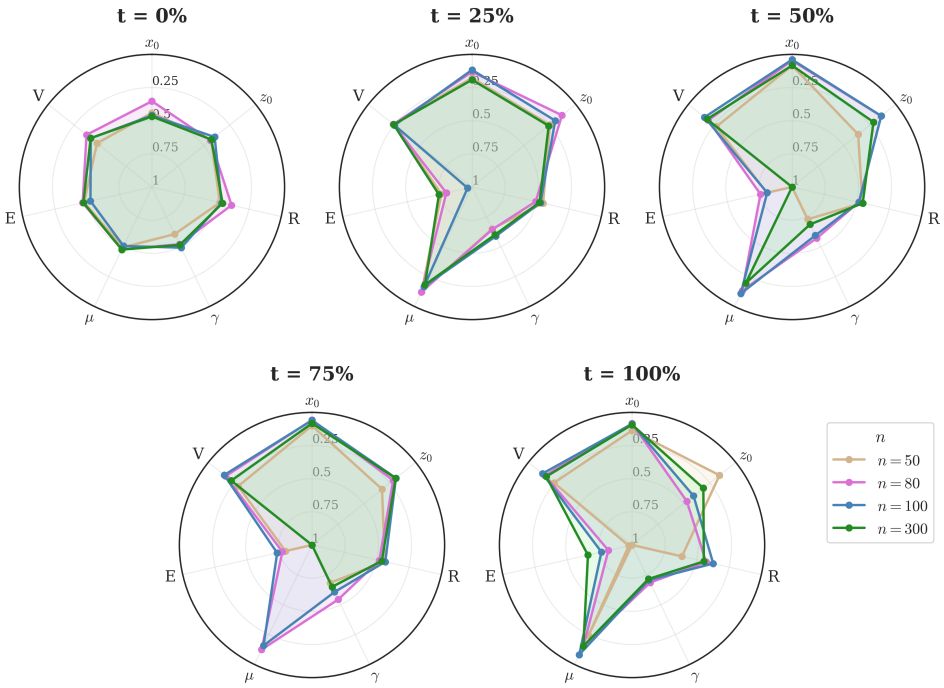


Figure S10: Radar diagrams showing the evolution of the models parameters accuracy over time in case of various numbers of particles. Results are obtained for $\Delta w = 1\%$ and $N_o = 600$. Normalized Mean Absolute Error is represented at various time steps, 0% (initial distribution before the assimilation starts), 25%, 50%, 75% and 100 %, of the time required for the magma to reach the surface for the synthetic truth.

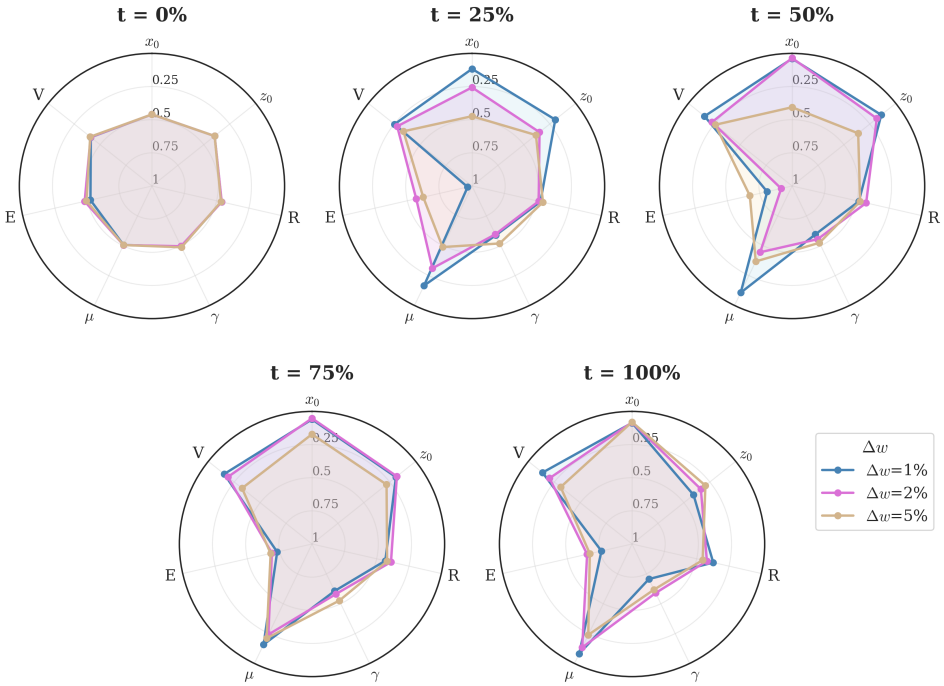


Figure S11: Radar diagrams showing the evolution of the models parameters accuracy over time in case of various assimilation windows. Results are obtained for $n = 100$ and $N_o = 600$. Normalized Mean Absolute Error is represented at various time steps, 0% (initial distribution before the assimilation starts), 25%, 50%, 75% and 100 %, of the time required for the magma to reach the surface for the synthetic truth.

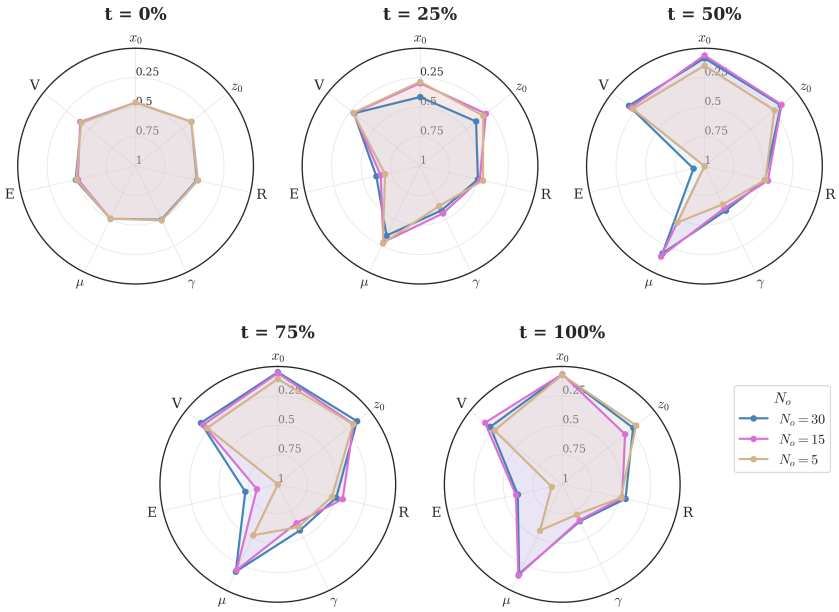


Figure S12: Radar diagrams showing the evolution of the models parameters accuracy over time in case of different number of observations. Results are obtained for $n = 100$ and $\Delta w = 1\%$. Normalized Mean Absolute Error is represented at various time steps, 0% (initial distribution before the assimilation starts), 25%, 50%, 75% and 100 %, of the time required for the magma to reach the surface for the synthetic truth. Observations are regularly spaced on the surface.

Copyright notice

References

Maccaferri, F., D. Smittarello, V. Pinel, and V. Cayol (2019). "On the Propagation Path of Magma-Filled Dikes and Hydrofractures: The Competition Between External Stress, Internal Pressure, and Crack Length". *Geochemistry, Geophysics, Geosystems* 20(4), pages 2064–2081. DOI: 10.1029/2018GC007915.

Smittarello, D., V. Pinel, F. Maccaferri, S. Furst, E. Rivalta, and V. Cayol (2021). "Characterizing the physical properties of gelatin, a classic analog for the brittle elastic crust, insight from numerical modeling". *Tectonophysics* 812, page 228901. DOI: 10.1016/j.tecto.2021.228901.

Watanabe, T., T. Masuyama, K. Nagaoka, and T. Tahara (2002). "Analog experiments on magma-filled cracks: Competition between external stresses and internal pressure". *Earth, Planets and Space* 54(12), pages 1247–1261. DOI: 10.1186/bf03352453.